Spatio–Temporal Imaging of Vascular Reactivity by Optical Tomography

Randall L. Barbour[1,3], Harry L. Graber[1], Christoph H. Schmitz[1], Yaling Pei[4], Sheng Zhong[3],
San–Lian S. Barbour[4], Seth Blattman[2], and Thomas Panetta[2]

Departments of [1]Pathology and [2]Surgery,
SUNY Downstate Medical Center, 450 Clarkson Ave., Box 25, Brooklyn, NY 11203

[3]Department of Electrical Engineering,
6 Metrotech Center, Polytechnic University, Brooklyn, NY 11201

[4]NIRx Medical Technologies Corp.
15 Cherry Lane, Glen Head, NY 11545

Abstract
Representative results from simulated, laboratory and physiological studies are presented, demonstrating the ability to extract important features of dynamic behavior from dense scattering media. These results were obtained by analyzing time series of reconstructed images. Investigations on the human forearm clearly reveal the ability to identify and correctly locate principal features of the vasculature. Characterization of these features using linear and nonlinear time–series analysis methods can produce a wealth of information regarding the spatio–temporal features of the dynamics of vascular reactivity.

Introduction
The vascular system is responsible for maintaining adequate perfusion of tissue. Perfusion states are modulated in response to local metabolic demands and central factors [1]. While various techniques have been developed to assess vascular perfusion, imaging methods increasingly are the preferred modality. Often assessment of perfusion is based either on measures that are sensitive to flow (*e.g.*, as determined by acoustic or optical Doppler measurements) or on anatomical evidence (*e.g.*, imaging studies that reveal the presence of stenosis). Certainly such measures have proven useful in many clinical situations. These, however, represent only a small faction of the information available regarding vascular dynamics. For instance, it is clear that various vascular beat frequencies exist and that these are attributable to different structures of the vascular tree (*e.g.*, a cardiac beat is restricted to the arteries, while a respiratory beat frequency occurs mainly in the microvessels). Presently, it is not possible to differentiate these signatures in a cross–sectional spatial map. Should this capability become available, it could prove especially useful for the early detection of disease processes that are known to compromise these responses (*e.g.*, onset of peripheral neuropathy in diabetes).

Other measures of vascular dynamics might also prove useful for diagnostic or monitoring purposes. For instance, blood flow within the arterial or venous structures is basically unidirectional. Within a selected cross–section, it may be expected that the pulsatile activity of the vasculature at a given frequency should be in phase. The presence of stenosis proximal to the measuring site could be indicated by either out–of–phase responses or significantly damped amplitudes. Spatial maps revealing either temporal correlations or the amplitude of a selected beat frequency could serve to identify lesions associated with inadequate perfusion.

Recently, we have demonstrated the ability to characterize dynamic features of dense scattering media and display this information in a cross–sectional view, by analyzing a time series of image data obtained by optical tomography [2,3]. These data were based on simulated hemodynamic models of the breast [2] and on laboratory studies of scattering media containing a dynamic phantom [2,3]. For this report we have extended these studies to include various measures of the dynamic response of the vasculature in the human forearm to simple physiological manipulation. Results obtained confirm the ability to identify well–known features of vascular dynamics (*e.g.*, the occurrence of cardiac and respiratory beat frequencies). Examples illustrating how simple linear time–series analysis methods can be used to locate and identify specific features of the vasculature tree also are given.

Methods
Target media: Three different target media have been explored. One of these involved numerical studies while the others involved experimental studies on a laboratory phantom or a human forearm.

i. Numerical Investigations: In this study we numerically modeled dynamic vascular behavior in a heterogeneous

tissue background. Our model was based on a segmented 2–D MRI image of the breast and included three different tissue types: adipose, parenchyma and a "tumor." By assigning appropriate values for the absorption coefficients we could model harmonic temporal fluctuations in tissue blood volume. The frequency of this modulation was varied in accordance to tissue type. The extent of modulation was ±10% about the mean value. The frequencies chosen were essentially arbitrary, but we did use values whose ratio closely matches the ratio of the cardiac to respiratory frequency found at rest. In an effort to simulate more realistic conditions, we also included in the model differences in tissue hemoglobin oxygenation levels and in values of the scattering coefficient. Variations in oxygenation levels were modeled by assigning absorption coefficient values that correspond to two different illumination wavelengths (760 and 840 nm). While the oxygenation level and scattering coefficient values differed for the different tissues, their temporal properties were time–invariant. Thus, our model simulated a dual–wavelength, time–varying tomographic measurement for which dynamic behavior was restricted to variations in blood volume. The external diameter of the breast phantom was 8 cm.

ii. Laboratory Phantom: The second case studied was a vessel, 7.6 cm in diameter, filled with 2% (v/v) Intralipid and containing two small balloons each filled with dilute (50 μM) solutions of hemoglobin. The balloons were made to beat at different frequencies by volumetric displacement using a piston pump. As with the hemodynamic tissue model, the specific frequencies chosen were arbitrary but their ratio closely matched the cardiac to respiratory beat frequency ratio at rest.

iii. Forearm studies: The third case examined involved dynamic measures on the human forearm. A range of responses have been explored, and include the influence of deep–breathing exercises, a cold shock, response to finger flexing, and influence of varying levels of restricting pressure produced by inflating a pressure cuff proximal to the measuring site. As our purpose here is only to demonstrate the fidelity and type of information retrievable from the time–series image data, we report only selected portions of these studies. Details of each of these will be reported at upcoming conferences [4] and elsewhere [5].

Collection of Time–Series Image Data: Tomographic data for the tissue model was acquired by using the finite element method to solve the diffusion equation with Dirichlet boundary conditions. The source/detector configuration used match those adopted in the experimental studies. In all cases, image formation was based on use of six source positions and eighteen detectors per source. Each source sequentially illuminated the target and data were collected in parallel. Sources were positioned uniformly about the target at 60° intervals, while detectors were positioned at 20° intervals. The sampling rate (simulated or real) varied depending on the experiment, but in all cases was 2–4 Hz. A total of 240–300 data points were collected for each time–series.

Instrumentation: Time–series detector data from experimental studies were collected using a recently described optical imager [3]. The instrument functions as a serial–source, multi–channel, parallel–detection device. Figure 1 show a photograph of the iris imaging head used in these studies. By adjusting the pass–through diameter, optical fibers can be brought into gentle contact with the target medium. Depending on the study, measurements were performed at 2–4 Hz in either a single– (810 nm) or dual–wavelength (780 and 810 nm) mode.
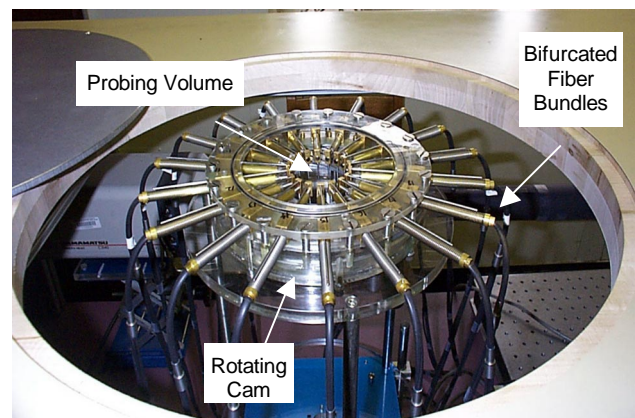

Figure 1: Photograph of iris imaging head.

Preimage Analysis and Image Reconstruction: For each detector channel, optical data at each time point were normalized to a mean value of the recorded signal. For most studies, the mean value was computed from the data points in the initial 30 s of measurement. The normalized values were then used as the input data vectors for image recovery. Images were computed by simultaneously solving for the diffusion and absorption coefficients using a recently described algorithm [6]. Computed solutions were limited to the first order Born approximation using a CGD solver. Also, while both coefficients were computed, reported results here are restricted to estimates of the absorption coefficient.

Post–reconstruction Image analysis: Where indicated, standard linear time–series analysis methods were employed to evaluate the image series [7]. For example, the frequency spectrum of the image time series was derived by computing the Fourier transform for each pixel. Other measures involved computing inter–pixel and detector–to–pixel cross–spectral density and coherence functions.

Results

Enhanced Image Contrast of Dynamic Features. Improvement in image contrast and resolution is important for any imaging method. Thus far, optical imaging methods have produced only images having relatively low contrast and resolution from tissue studies. While refinements in data processing and instrument performance may improve this situation, at this point it would seem that these contrast and resolution levels might represent basic features of optical imaging. Recently we have shown [2,3] that images that identify *dynamic behavior* in the optical coefficients (*e.g.*, amplitude of time–harmonic oscillations in μ_a) can produce spatial maps that have greatly improved quality compared to images of the spatial contrast in the optical coefficients *per se*. These can include amplitude and phase maps of the Fourier spectrum, and maps of temporal correlations and their frequency composition. As an example, in Figure 2 we show an original image of a complex target medium (a), a reconstructed map of its time–averaged blood volume levels (b), and a map of the computed coherence at a selected frequency (c) computed from the same data shown in (b) and derived from analysis of a time series.
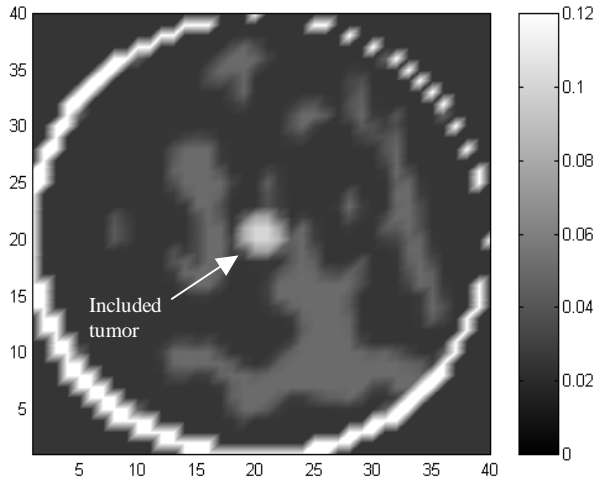

Figure 2. Panel A. Contrast map of simulated blood volume levels in MR mammogram. Panel B, reconstructed time–averaged image of blood volume. Panel C, computed coherence between an indicated index pixel ('x') and image map. Scale in panels A and B indicate fractional blood volume in tissue. Modeled blood volume levels were: adipose tissue (black) – 2.5%, parenchymal tissue (dark gray) – 3.5%, tumor (light gray) – 10%; oxygen saturation levels were: adipose tissue – 100%, parenchymal tissue – 90%, tumor – 50%; modulation frequencies were: adipose tissue – 0.12 Hz, parenchymal tissue – 0.40 Hz, tumor – 0.06 Hz. The map shown in panel C is the 0.35 Hz component of the coherence function.

The original is a 2–D coronal section of a MR mammogram, for which various optical properties ($0.04 < \mu_a < 0.3$, $5 < \mu_s < 15$ cm^{-1}) were assigned to the different tissue types [adipose (dark), parenchyma (gray) and tumor (light)] (see legend for description). Comparison shows

the resolution and contrast of the time–averaged map is

B. Reconstructed map of blood volume
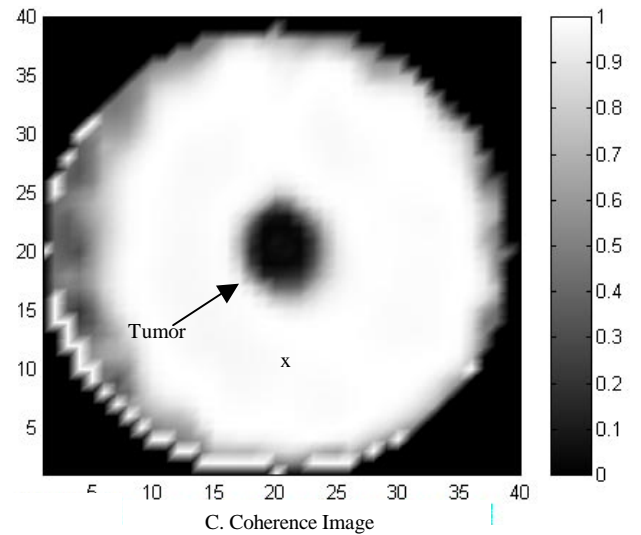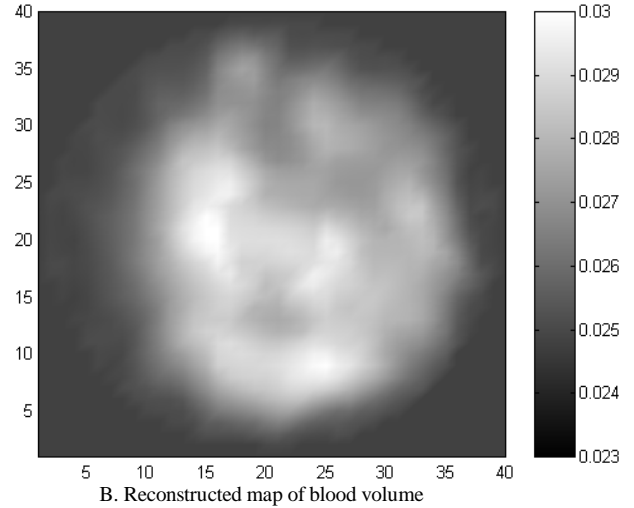
C. Coherence Image

relatively low and the tumor is not evident. In contrast, the tumor is clearly revealed in the coherence image. Significantly, this result was obtained without any prior knowledge of the tumor's presence, and instead is dependent solely on the tumor having a *temporal* response different from that of the surrounding tissue. Clinically, such behavior may exist naturally [8], or it could be induced in response to a simple manipulation of the vascular perfusion state. These findings thus demonstrate that high–quality image data revealing the presence of dynamic behavior in a dense scattering medium can be derived from analysis of time series of images of a complex simulated phantom. Next we show results demonstrating that images of similar quality can be obtained from a laboratory phantom exhibiting dynamic behavior.

Spatio–Temporal Imaging of a Dynamic Phantom. Figure 3 shows a schematic of the apparatus used for the phantom

study. Illustrated are two balloons filled with a dilute solution of hemoglobin (50 μM) and attached to a support structure. The balloons are made to beat at different frequencies by periodic volume displacement.
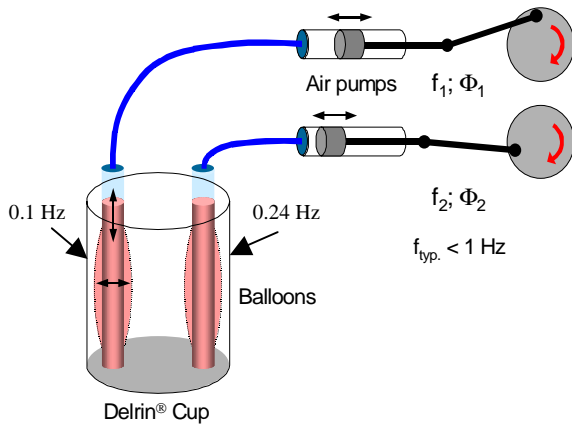

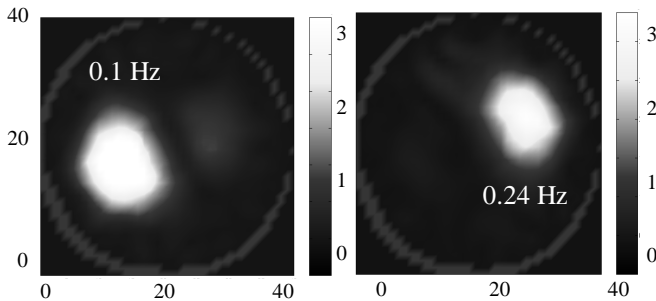Figure 3. Schematic of apparatus used for dynamic phantom study.

Figure 4. Reconstructed FT image of oscillating balloons.

The apparatus was introduced into a vessel 7.6 cm in diameter and containing 500 mL of 2% (v/v) Intralipid. Time–series tomographic measurements were performed using the iris imaging head shown in Figure 1. Figure 4 shows images derived by computing the Fourier transform of the image series at the two different beat frequencies. Inspection reveals nearly complete spatio–temporal resolution of the added inclusions.

Imaging of Dynamic Behavior of Vascular Reactivity in the Human Forearm.

The natural occurrence of vascular frequencies arising from respiratory and cardiac activity can be exploited to produce a spatial map revealing the presence of different components of the vascular tree. Figure 5 shows a map of the logarithm of the ratio of the computed FT amplitudes at the cardiac and respiratory frequencies obtained from a time–series measurement on the forearm. Figure 6 is a representative MR image in the same region of forearm. An overlay of the two maps having the same orientation is shown in Figure 7. Inspection reveals that in the vicinity of the radial (1), interosseous (3) and ulnar (5) arteries, the

ratio of the Fourier amplitudes (cardiac to respiratory) is nearly ten times larger than it is in other regions.
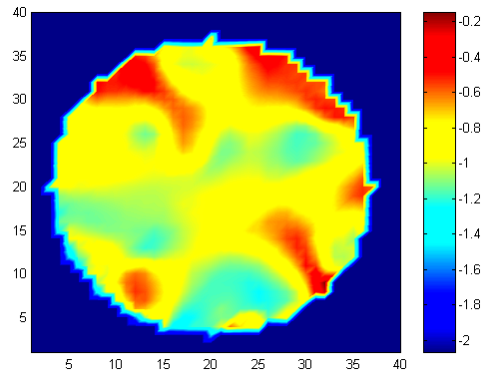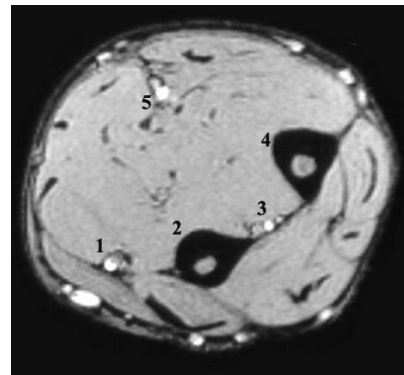

Figure 5. Map of ratio of FT amplitude.

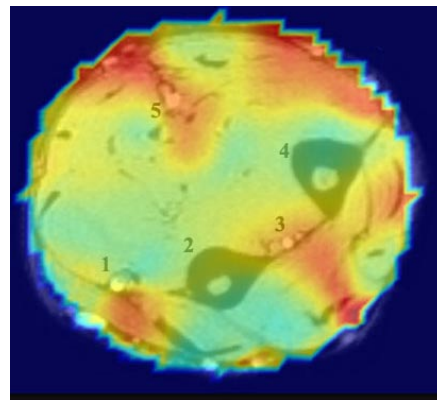Figure 6. MR image of forearm. (1) radial artery,(2) radius, (3) interosseous artery, (4) ulna, (5) ulnar artery.

Figure 7. Overlay image.

This response can be seen more clearly in Figure 8, which shows the cross–spectral density (CSD) between a surface detector and specific locations in the image. The particular spectra shown were obtained from points in the image corresponding to locations in the flexor digitorum superficialis muscle, and points near the radial and interosseous arteries. Inspection reveals that in muscle the dominant signal coincides with the frequency of

respiration, while for the arteries the dominant signal is at the cardiac frequency.
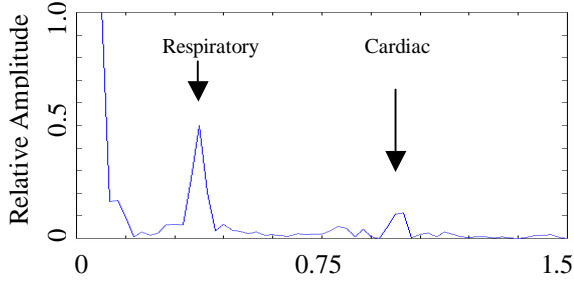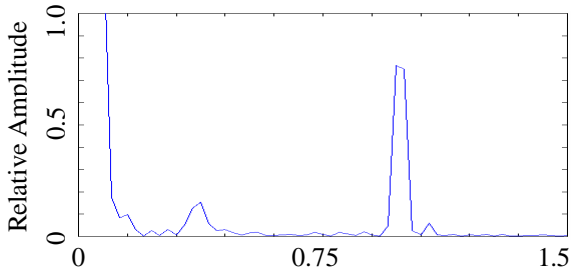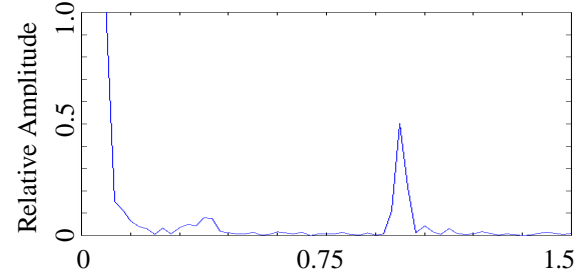

Figure 8. Panel A. CSD spectrum at position (19, 12)

Panel B. CSD spectrum at position (11, 13)

Panel C. CSD spectrum at position (18, 27)

Finger–Flex study.

In this study we further explored the ability to measure dynamic behavior by examining an image time series derived from measurements obtained while the subject was conducting a finger–flex exercise. Finger flexing involves the action of so–called antagonistic muscle groups that are located on opposite sides of the forearm, specifically the flexor digitorum superficialis on the ventral side and the extensor digitorum on the dorsal side. Results in Figure 9, panel A show a map of the amplitude of the Fourier spectrum obtained at the finger–flex frequency (0.25 Hz). Figure 9, panel B shows an overlay of this image onto an MR image of the same forearm oriented in the same position. Inspection reveals that positions of maximum amplitude for finger–flexing coincide well with the two involved muscle groups.

Further evidence supporting the accuracy of this assignment is shown in Figure 10. Shown are time series values for μ_a at points in the image coinciding with the involved muscles. It is noteworthy that the two signals are approximately 180° out of phase with each other, which is the expected response from the action of antagonistic muscle groups.
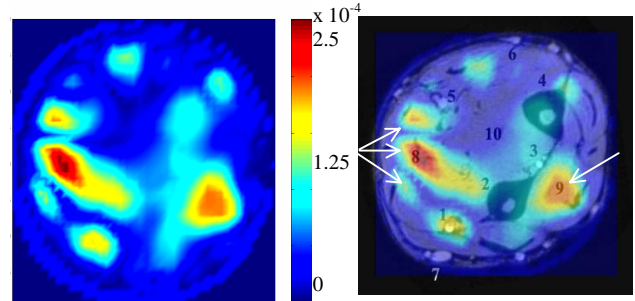

Figure 9. Panel A. Map of amplitude of FT at the finger–flex frequency. Panel B. Overlay image with identified anatomic structures: 1), radial artery, 2) radius, 3) interosseous artery, 4) ulna, 5) ulnar artery, 6) basilic vein, 7) cephalic vein, 8) flexor digitorum superficialis, 9) extensor digitorum, 10) flexor digitorum profundus. Arrows indicate areas regions that overlay on involved muscle groups.
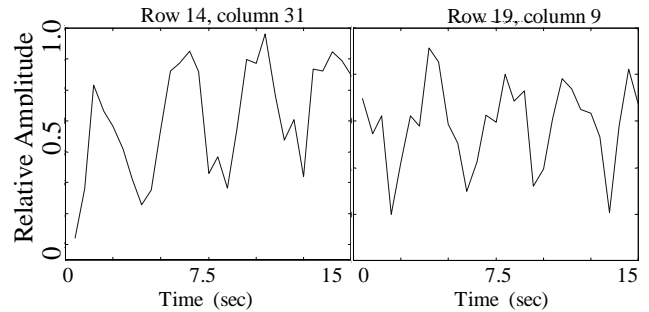

Figure 10. Temporal variations in μ_a at pixel locations in involved muscle groups.

Discussion

A hallmark of vascular system is the rapidity and flexibility of its responses to changing metabolic demands. This is accomplished through the dynamic interaction of local metabolic and central neurological control mechanisms. Currently, our ability to investigate these interactions is primarily limited to discrete measures of flow in large deep vessels or small superficial vessels. Lacking is a comprehensive understanding of the integrated physiological response of vascular reactivity, whose details will certainly vary with anatomical site and disease states. As has been abundantly demonstrated by electrocardiographic and electroencephalographic studies, much information about physiological response and control can be gained by examination of time–varying processes. We believe this insight regarding the control of vascular reactivity is attainable by optical tomography. In this report we presented results documenting the ability to measure specific time–varying features in a range of target media. Examined were various features identifiable using linear time–series analysis methods. While these measures can provide a valuable insight regarding vascular dynamics, there is much evidence indicating that nonlinear

processes govern the vascular response. In this regard we have recently demonstrated the ability to detect temporal fluctuations in optical properties defined by a chaotic time series, and to differentiate these from harmonic, quasiperiodic, and stochastic responses [9]. Extension of this capability to physiological studies could open new vistas in our understanding the vascular response and aid in the design of rational treatment protocols for disease intervention.

References
1. J. B. West, Ed., *(Best and Taylor's) Physiological Basis of Medical Practice*, 11/e, Williams & Wilkins, 1985.
2. R. L. Barbour, H. L. Graber, Y. Pei, S. Zhong, C. H. Schmitz, J. Hira, I. Arif, "Optical tomographic imaging of dynamic features of dense–scattering media," *J. Opt. Soc. Am. A*, submitted.
3. C. H. Schmitz, H. L. Graber, H. Luo, I. Arif, J. Hira, Yaling Pei, A. Bluestone, S. Zhong, R. Andronica, I. Soller, N. Ramirez, S.–L. S. Barbour, R. L. Barbour, "Instrumentation and calibration protocol for imaging dynamic features in dense–scattering media by optical tomography," *Appl. Opt.*, submitted.
4. Advances in Optical Imaging and Photon Migration, OSA Biomedical Topical Meetings, Apr. 2–5, 2000; Physiology and Function from Multidimensional Images, SPIE Medical Imaging 2000 Symposium, Feb. 13–15, 2000.
5. R. L. Barbour, H. L. Graber, Y. Pei, C. Schmitz, and S. Zhong, manuscripts in preparation.
6. Y. Pei, F.–B. Lin, and R. L. Barbour, "Model–based imaging of scattering media using relative detector values," *Optics Express*, submitted.
7. J. S. Bendat and A. G. Piersol, *Engineering Applications of Correlation and Spectral Analysis*, 2/e, John Wiley & Sons (New York), 1993.
8. T. M. Griffith, "Chaos and fractals in vascular biology," *Vasc. Med. Rev.*, Vol. 5, pp. 161–182, 1994.
9. R. L. Barbour, H. L. Graber, Y. Pei, C. Schmitz, and S. Zhong. "Spatio–Temporal Imaging of Vascular Reactivity" *Nature*, submitted.